Check for updates

Formation of a low-symmetry Pd$_8$ molecular barrel employing a hetero donor tetradentate ligand, and its use in the binding and extraction of C$_{70}$†

Dharmraj Prajapati,[a] Jack K. Clegg [ID][b] and Partha Sarathi Mukherjee [ID] *[a]

The majority of reported metallo-supramolecules are highly symmetric homoleptic assemblies of M$_x$L$_y$ type, with a few reports on assemblies that are obtained using multicomponent self-assembly or using ambidentate ligands. Herein, we report the use of an unsymmetrical tetratopic ligand (L^{un}) containing pyridyl and imidazole donor sites in combination with a *cis*-protected Pd(II) acceptor for the formation of a low-symmetry M$_8$L$^{un}_4$ molecular barrel (**UNMB**). Four potential orientational isomeric (HHHH, HHHT, HHTT, and HTHT) molecular barrels can be anticipated for the M$_8$L$^{un}_4$ type metallo-assemblies. However, the formation of an orientational isomer (HHTT) of the barrel was suggested from single-crystal X-ray diffraction and ^{1}H NMR analysis of **UNMB**. Two large open apertures at terminals and the hydrophobic confined space surrounded by four aromatic panels of L^{un} make **UNMB** a potential host for bigger guests. **UNMB** encapsulates fullerenes C$_{70}$ and C$_{60}$ favoured by non-covalent interactions between the fullerenes and aromatic panels of the ligand molecules. Experimental and theoretical studies revealed that **UNMB** has the ability to bind C$_{70}$ more strongly than its lower analogue C$_{60}$. The stronger affinity of **UNMB** towards C$_{70}$ was exploited to separate C$_{70}$ from an equimolar mixture of C$_{70}$ and C$_{60}$. Moreover, C$_{70}$ can be extracted from the C$_{70}$⊂**UNMB** complex by toluene, and therefore, **UNMB** can be reused as a recyclable separating agent for C$_{70}$ extraction.

Introduction

Nature has used various types of non-covalent interactions to control the preciseness of self-assembly processes to ensure that the individual components combine in specific ratios and orientations to function effectively.[1] For instance, protein-based enzymes convene into homo- or hetero-polymeric quaternary structures to execute a variety of biological functions.[2] The active sites of these enzymes are enclosed by low symmetrical and chiral cavities containing a combination of different chemical functionalities, such as catalytic sites, recognition sites, and conformational switches.[3] Over the past few decades, chemists across the globe in different fields have tried to imitate these principles by applying them to synthetic systems.[4] In this regard, a wide range of supramolecular architectures, such as self-assembled coordination cages,[5] molecular capsules,[6] and molecular barrels[7] that demonstrate a vast range of important

applications, have been developed.[8] Nonetheless, the majority of such self-assembled molecules reported to date are highly symmetric and homoleptic complexes of M$_x$L$_y$ type, which were prepared by incorporating a selected metal node (M) and only one type of symmetric ligand (L).[5–8] Recently, there has been a push towards unfolding lower symmetry systems intending to get upgraded functionally. In addition to heading towards supramolecular assemblies with reduced symmetry,[9] such as heteroleptic cage systems[10] and hetero-polymetallic cage systems,[11] there has also been a rise in interest in developing self-assembled systems containing bis-monodentate ligands of two different donor groups.[12] However, unsymmetrical multi-topic ligands (number of donor sites > 2) with distinct binding sites remain largely ignored because of the possibility of the formation of a mixture of different isomers. An isomeric mixture of the complexes might be formed due to the random relative orientational arrangement of the ligands around the metal centres. Thus, selecting an unsymmetrical ligand with distinct donor sites for the synthesis of self-assembled coordination complexes of lower symmetry is quite challenging.

Fullerene is one of the stable allotropes of carbon and has a vast range of captivating properties, such as conducting, magnetic, antioxidant, and electronic, due to its unusual symmetry and extended conjugated electronic features.[13] Owing to these properties, fullerenes find applications in several fields, for instance in materials science,[14] in superconducting

[a]*Department of Inorganic and Physical Chemistry, Indian Institute of Science, Bangalore-560012, India. E-mail: psm@iisc.ac.in*

[b]*School of Chemistry and Molecular Biosciences, The University of Queensland, St. Lucia, Queensland 4072, Australia*

materials,[15] as electroactive materials in solar cells,[16] and for biological applications.[17] However, these applications largely depend on their purity and solubility. Unrefined carbon soot contains a mixture of fullerenes of different carbon numbers and amorphous forms of carbon and other allotropes such as carbon nanotubes.[18] The popular purification techniques to separate fullerenes from carbon soot are recrystallization, controlled sublimation, and extraction with organic solvents.[19] In recent times, chromatographic methods have been used predominantly for the isolation and purification of fullerenes.[20] Although efficient columns are available for the isolation of fullerene using HPLC techniques, all of these purification methods need large amounts of solvents and can induce irreversible adsorption, and decomposition of fullerene within the column.[20] Moreover, these techniques are often expensive, tedious, energy and time-consuming, and in some instances, it is difficult to get a particular fullerene with high selectivity. Therefore, inventing techniques for the purification of fullerenes is a challenging and highly desirable task in materials chemistry. Over the past few decades, selective separation of fullerenes by encapsulation within soluble supramolecular receptors has attracted the research community's attention[21] because this method offers potential selectivity *via* selective host–guest complexation without any special equipment. Moreover, the encapsulation of fullerene enhances its solubility. Therefore, it is highly appealing to devise a suitable molecular host that has a better binding affinity for one fullerene over the other, leading to their separation from a mixture.

Herein, we report the formation of an unsymmetrical molecular barrel (**UNMB**) of $M_8L^{un}_4$ type by coordination-driven self-assembly of an unsymmetrical tetratopic donor 4′-(3,5-di(1*H*-imidazol-1-yl)phenyl)-4,2′:6′,4″-terpyridine (**L^{un}**) containing pyridine and imidazole donor sites with *cis*-[(tmeda) Pd(ONO$_2$)$_2$] as an acceptor in DMSO (tmeda = N,N,N',N'-tetramethyl-ethane-1,2-diamine) (Scheme 1). The orientational isomeric product (**UNMB**) was characterized by ^{1}H NMR, 2D DOSY NMR, and ESI-MS analysis. Furthermore, the molecular structure was unambiguously established by single-crystal X-ray

diffraction analysis. **UNMB** features a rhombohedral hydrophobic cavity fenced by extended π-conjugated aromatic rings of the four ligand units (**L^{un}**) along with two large open windows. Above-mentioned features of **UNMB** assist the encapsulation of C_{70} and C_{60} inside its hydrophobic cavity. ESI-MS analysis of $C_{70} \subset$ **UNMB** and $C_{60} \subset$ **UNMB** revealed the formation of 1 : 1 host–guest complexes (Scheme 1). Furthermore, association constant values (K_a), DFT studies, and competitive guest encapsulation studies suggested that **UNMB** has better binding affinity towards C_{70} over C_{60}, which enables the recyclable separation of C_{70} from an equimolar mixture of C_{60} and C_{70}.

Results and discussion

Synthesis and characterization of UNMB

The new tetratopic unsymmetrical ligand **L^{un}** containing two imidazole and two pyridyl donor sites was synthesized by standard Ullman coupling of 4′-(3,5-dibromophenyl)-4,2′:6′,4″-terpyridine with imidazole (Scheme S1†).[20] Ligand **L^{un}** was characterized by ^{1}H and ^{13}C NMR spectroscopy (Fig. S2–S5†). A mixture of ligand **L^{un}** (1 equivalent) and metal acceptor *cis*-[(tmeda)Pd(ONO$_2$)$_2$] (**M**) (2 equivalents) in DMSO was heated for 12 h at 60 °C under stirring. Afterward, the resulting clear solution was precipitated by treating it with an excess of ethyl acetate. The precipitate was centrifuged and dried under vacuum to get a white powder of **UNMB** in 98% yield. The obtained white powder of **UNMB** was analysed by NMR and ESI-MS spectroscopy. Due to the unsymmetrical nature of the tetratopic donor **L^{un}**, upon self-assembly with 90° acceptor **M**, it may produce different orientational isomers of the most common compositions, such as $M_6L^{un}_3$ or **$M_8L^{un}_4$**. The ^{1}H NMR spectrum of **UNMB** in D$_2$O displayed a set of eight peaks in the aromatic region and three signals each for ethylene and methyl protons of the acceptor unit in the aliphatic region (2.6–3.3 ppm) (Fig. 1, S6 and S7†). The integral ratio (1 : 2 : 1) of the proton signals of ethylene and methyl groups in the aliphatic
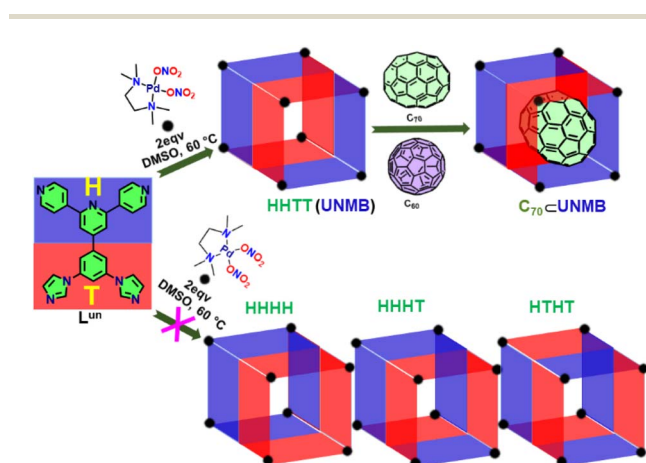
Scheme 1 Schematic presentation of the synthesis of unsymmetrical molecular barrel UNMB, and its selective encapsulation of C_{70}.
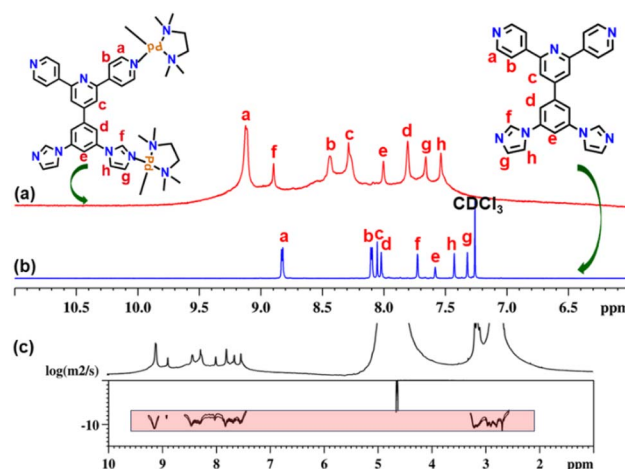

Fig. 1 Stacked partial ^{1}H NMR spectra of (a) **UNMB** in D$_2$O, (b) ligand **L^{un}** in CDCl$_3$, and (c) diffusion-ordered ^{1}H NMR of **UNMB** in D$_2$O.

region probably hints at either the formation of the product that has three different kinds of (tmeda)Pd(II) units in a 1 : 2 : 1 ratio (Fig. S8†) or an equilibrium mixture. Moreover, a significant downfield shift was observed in the signals of pyridyl α-protons (H$_a$) and imidazole protons (H$_f$) with $\Delta\delta = 0.33$ and $\Delta\delta = 1.16$ ppm, respectively, which indicates the formation of ligand-to-metal dative bonds (Fig. 1 and S6†). Additionally, the appearance of a single diffusion band in the 2D DOSY (diffusion order spectroscopy) NMR spectrum indicated the formation of a single self-assembled molecular architecture (Fig. 1c and S8†). Moreover, all the proton signals of **UNMB** were assigned by a thorough investigation of ^1H–^1H COSY NMR, which confirmed that all signals are originated from the ligand **L^{un}** (Fig. S9†). Thus, altogether, the NMR spectral data provided preliminary information in support of the formation of a self-assembled architecture, but due to the absence of the required splitting patterns of the proton signals, it could not suggest the arrangement of the donors in the final assembly.

The molecular composition of the self-assembled molecular architecture in solution was ascertained by electrospray ionization mass spectroscopy (ESI-MS). For this, an aqueous solution of **UNMB** was reacted with an excess of KPF$_6$ at room temperature overnight. The ESI-MS spectrum of the PF$_6^-$ analogue was recorded in acetonitrile. The ESI-MS spectrum showed the presence of several noticeable peaks and respective isotopic distribution patterns corresponding to the charge fragments at $m/z = 1810.4826$ for $[M_8L^{un}_4(PF_6)_{13}]^{3+}$, 1321.6334 for $[M_8L^{un}_4(PF_6)_{12}]^{4+}$, 1028.3242 for $[M_8L^{un}_4(PF_6)_{11}]^{5+}$, 832.7648 for $[M_8L^{un}_4(PF_6)_{10}]^{6+}$, and 693.0971 for $[M_8L^{un}_4(PF_6)_9]^{7+}$, which are well matched with the respective calculated isotopic distribution patterns of the above mentioned charged fragments (Fig. 2, S11 and S12†). Thus, ESI-MS investigation suggested the

formation of a molecular architecture with the composition of **M$_8$L$^{un}_4$**.

Due to the different orientations of four molecules of non-symmetric ligand **L^{un}**, several orientational isomeric barrels like HHHH, HHHT, HHTT and HTHT (Scheme 1) are possible. In the case of the most symmetric HHHH (having C_{4V} symmetry) isomer, there will be two kinds of palladium centres in a 1 : 1 ratio. One set of Pd ions will be coordinated to the pyridyl units and another set will be connected with the imidazole units; hence, in this case, the ^1H NMR pattern will presumably be simpler.[7e,f] However, in the case of the HTHT (having D_{2d} symmetry) isomer, there will be only one kind of Pd(II) centre; hence, each pyridyl and imidazole unit will face an identical electronic environment, and therefore, again, a much simple NMR pattern is expected. The aliphatic proton peaks' integrations in a ratio of 1 : 2 : 1 hint at the formation of either the HHTT (having C_{2v} symmetry) or HHHT (having C_s symmetry) isomer. Only these two isomers have three different kinds of (tmeda)Pd(II) units. ^1H NMR data in combination with the ESI-MS result indicated the formation of one of these isomers.

A computational study was performed to determine the comparative stabilities of these isomeric barrels, depicted in Scheme 1. Initially, the computational optimization for all the isomers was performed by the PM6 semiempirical method in their ground state. Next, single point energy calculations were carried out by employing the DFT method (B3LYP/LanL2DZ, 6-31G). From the DFT calculations, it can be observed that orientational isomer HHHH is found to be the energetically most favoured isomer, while isomer HTHT is the least favourable (Fig. 3). However, the energy difference among the HHHH, HHHT and HHTT isomers was found to be small (<20 kcal mol^{-1}) (Table S2†). Moreover, the energy difference between the HHTT and HHHT isomers (one of which is indicated to be formed by ^1H NMR analysis) is almost negligible. Thus, the theoretical study did not give enough information to predict the isomer formed.

Although ^1H NMR and ESI-MS analyses gave a preliminary idea about the formation of a **M$_8$L$^{un}_4$** barrel, such studies could not predict the actual isomer formed. Therefore, to get precise information about the isomer formed, a single-crystal X-ray diffraction study was necessary. To do this, suitable single crystals were grown by slow diffusion of acetone vapour into an aqueous solution of **UNMB** at room temperature. The diffraction study was carried out with a synchrotron beam line.[22] The
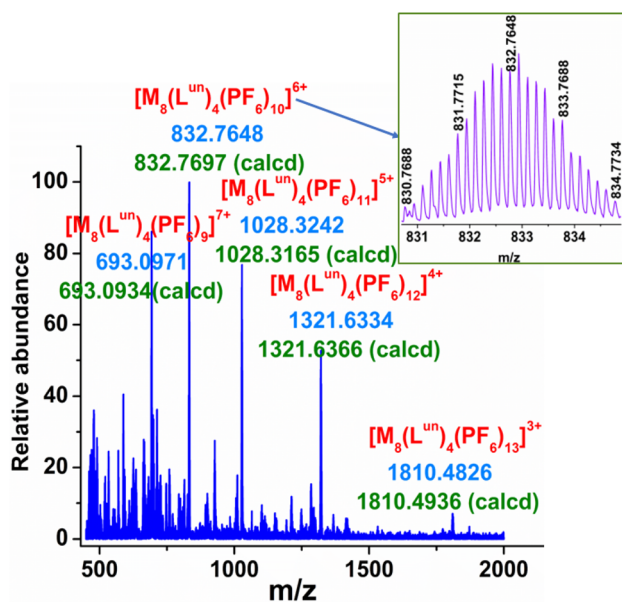

Fig. 2 ESI-MS spectrum of the PF$_6^-$ analogue of **UNMB** in acetonitrile. (Inset) Experimental isotopic distribution pattern of the $[M_8L^{un}_4(PF_6)_{10}]^{6+}$ fragment.
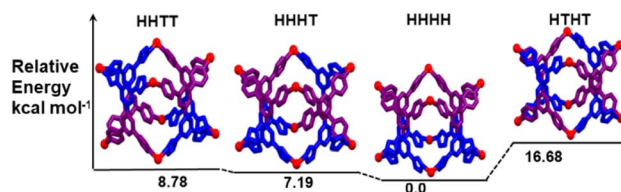

Fig. 3 Energy level diagram with the DFT [B3LYP/LanL2DZ, 6-31G] geometry optimized structures in the gas phase for the four possible linkage isomers of the $[Pd_8(L^{un})_4]^{16+}$ complex.

single crystal data unequivocally revealed the formation of the HHTT isomer (Fig. 4).

The Pd_8 barrel crystallized in the triclinic system with space group $P\bar{1}$ and two molecules were found in the asymmetric unit. The crystal structure of **UNMB** revealed that there are three types of Pd(tmeda) units present in **UNMB**. Two Pd centres (labelled as Pd1 and Pd1$'$) out of eight relate to only imidazole rings and other set of Pd centres (labelled as Pd2 and Pd2$'$) are coordinated only with pyridine units, whereas remaining four Pd ions (labelled as Pd3, Pd3$'$, Pd3$''$, and Pd3$'''$) are each bound to one imidazole unit and one pyridine ring. This mode of coordination bonding between the Pd(tmeda) centres and imidazole/pyridine units of L^{un} resulted in orientational self-sorting type self-assembly and gave rise to the formation of the HHTT isomer. The presence of three different types of (tmeda)Pd(II) units in the single crystal structure of **UNMB** thus supports the findings of the ^1H NMR data. Moreover, the redissolved crystals gave a very clean ^1H NMR spectrum, which exactly matches that of the as synthesized barrel **UNMB**. This finding further gives primary evidence for the formation of the HHTT isomer in solution. Therefore, single-crystal XRD analysis confirmed the formation of the low symmetry barrel HHTT. The average distance between the Pd(II) ions in opposite corners is ~21.25 Å for Pd1–Pd2$'$ and ~15.65 Å for Pd3–Pd3$''$; however, the distance between the adjoining Pd centres is roughly ~12.67 Å.

Fullerene encapsulation studies

Two large open terminal windows and the hydrophobic cavity enclosed by the aromatic rings of four ligands make **UNMB** a suitable encapsulant for the entrapment of large guest molecules. Therefore, to investigate the guest binding ability of **UNMB**, we chose large sized insoluble guests C_{60} and C_{70}. An aqueous solution (0.5 mL) of **UNMB** was stirred with 2

equivalents of fullerene C_{60} for 12 h at 55 °C, but the resultant solution showed no colour change. ^1H, ^{13}C and ESI-MS spectra showed the spectral data corresponding to only free **UNMB**. Evidently, there is no interaction between C_{60} and the host in an aqueous medium. Moreover, stirring C_{70} and **UNMB** did not result in any change in the spectral features, indicating no encapsulation of C_{70} either in an aqueous medium. Stunningly, when two equivalents of solid C_{60} were added to the acetonitrile solution of **UNMB** (PF_6-analogue) and heated at 55 °C under stirring, the colour of the reaction mixture slowly changed to light violet within 2 h and it got darker after completion of the reaction. The resulting suspension was centrifuged, and the supernatant was examined by ESI-MS, ^1H and ^{13}C NMR and electronic absorption spectroscopy. As C_{60} is insoluble in acetonitrile, the appearance of the characteristic profile in the spectroscopic data suggested the binding of C_{60} with **UNMB** in an acetonitrile medium. In contrast to the sharp and simple signals in the ^1H NMR spectrum of the free **UNMB** host, $C_{60} \subset$ **UNMB** displayed multiple signals suggesting strong enough interaction between the guest C_{60} and host **UNMB** (Fig. S13†). Additionally, a single horizontal band in the DOSY NMR spectrum revealed that all the signals belong to a single species (Fig. S14†). Moreover, a sharp and intense signal at 142 ppm was obtained in the ^{13}C NMR spectrum of $C_{60} \subset$ **UNMB** due to C_{60}, which further confirms the binding of C_{60} with **UNMB** (Fig. 5 and S15†).

In line with this, the ESI-MS spectrum showed several peaks corresponding to charge fragments associated with host–guest complex $C_{60} \subset$ **UNMB**. The isotopic distribution pattern corresponded to charge fragments at $m/z = 1501.6285$ for $[C_{60} \subset UNMB(PF_6)_{12}]^{4+}$, 1172.3069 for $[C_{60} \subset UNMB(PF_6)_{11}]^{5+}$, 952.7668 for $[C_{60} \subset UNMB(PF_6)_{10}]^{6+}$, 795.9456 for $[C_{60} \subset UNMB(PF_6)_9]^{7+}$, and 678.3319 for $[C_{60} \subset UNMB (12PF_6)_8]^{8+}$ (Fig. 6, S16 and S17†), suggesting the formation of a host–guest adduct with the stoichiometry of 1 : 1. These isotopic distribution patterns matched well with the simulated isotopic distribution pattern for the respective charge fragments. Furthermore, the ESI-MS spectrum of the $C_{60} \subset$ **UNMB** adduct
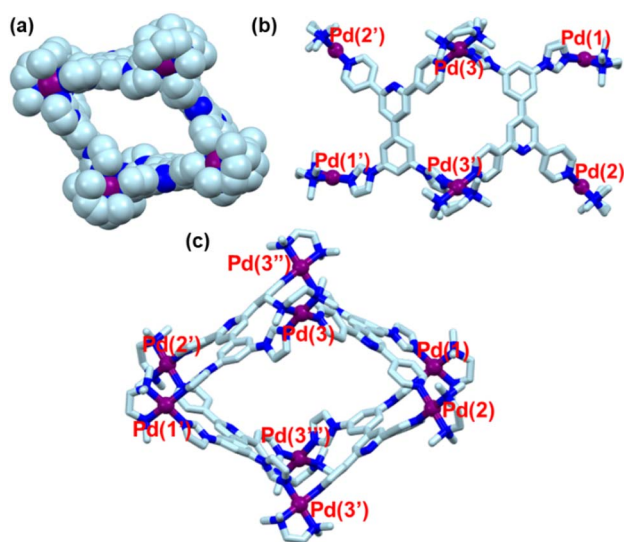

Fig. 4 SC-XRD structure of **UNMB**: (a) space-filling diagram; (b) side view; (c) top view (capped stick model) [color codes: C (light blue), N (blue), Pd (purple)]. Counter anions, hydrogen atoms, and solvent molecules have been omitted for the sake of clarity.
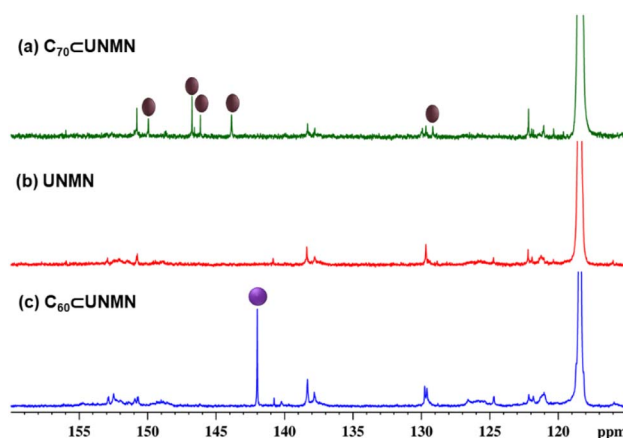

Fig. 5 Stacked partial ^{13}C NMR spectra of (a) $C_{70} \subset$ **UNMB**, (b) **UNMB**, and (c) $C_{60} \subset$ **UNMB** recorded in CD_3CN at room temperature.
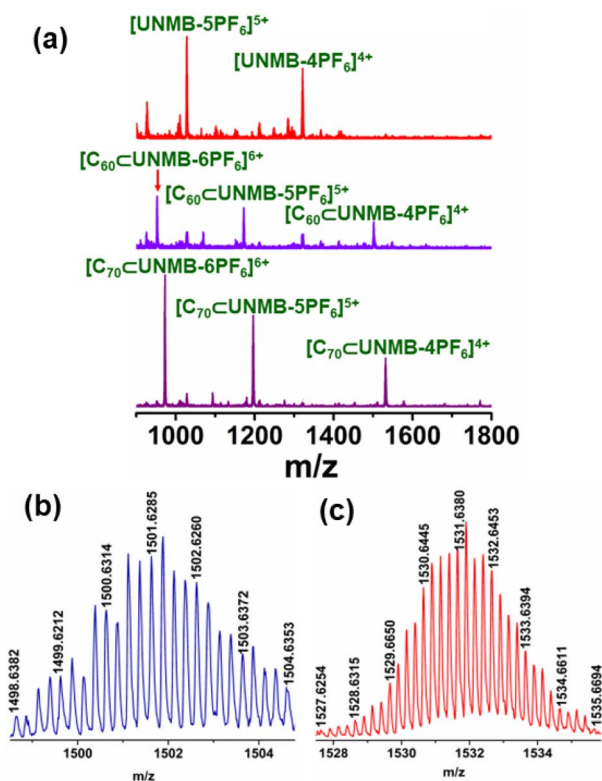
Fig. 6 (a) Stacked partial ESI-MS spectra of **UNMB** (red), $C_{60} \subset$**UNMB** (violet), and $C_{70} \subset$**UNMB** (purple). Experimental isotopic distribution patterns of (b) $[C_{60} \subset$**UNMB**$(PF_6)_{12}]^{4+}$, and (c) $[C_{70} \subset$**UNMB**$(4PF_6)_{12}]^{4+}$ fragments in ESI-MS.

showed the presence of peaks for free **UNMB** in addition to the signals for $C_{60} \subset$**UNMB**. This is owing to the decomplexation of the host–guest adduct at the time of ionization.

Similarly, host–guest complexation was performed employing C_{70} as a guest. A colourless acetonitrile solution of **UNMB** was treated with two equivalents of solid C_{70} at 55 °C under stirring, which resulted in a deep purple suspension after 12 h. After removal of the excess guest, the deep purple solution was analysed with various spectroscopic methods. Like $C_{60} \subset$**UNMB**, $C_{70} \subset$**UNMB** displayed multiple peaks in the ^{1}H NMR spectrum (Fig. S18†); however, the single diffusion band in DOSY NMR spectroscopy revealed that all the signals are associated with a single species (Fig. S19†). Interestingly, five additional signals at 149.55, 146.59, 146.15, 143.87 and 129.16 ppm appeared in the ^{13}C NMR of the $C_{70} \subset$**UNMB** complex (Fig. 3 and S20†), contrary to the single extra peak in the case of the $C_{60} \subset$**UNMB** adduct. The appearance of these new peaks is due to the presence of chemically different carbon atoms in C_{70},[22] and the presence of these additional resonance peaks strongly suggests the formation of an inclusion complex of **UNMB** with C_{70}.

The ESI-MS spectrum of $C_{70} \subset$**UNMB** showed six isotopically well resolved peaks at m/z = 2090.5246, 1531.6380, 1196.3206, 972.7755, 813.0999 and 693.3494 corresponding to charge fragments $[C_{70} \subset$**UNMB**$(PF_6)_{13}]^{3+}$, $[C_{70} \subset$**UNMB**$(PF_6)_{12}]^{4+}$, $[C_{70} \subset$**UNMB**$(PF_6)_{11}]^{5+}$, $[C_{70} \subset$**UNMB**$(PF_6)_{10}]^{6+}$, $[C_{70} \subset$**UNMB**$(PF_6)_9]^{7+}$, $[C_{70} \subset$**UNMB**$(PF_6)_8]^{8+}$, respectively (Fig. S21

and S22†). The isotopic distribution pattern of these peaks resembled the theoretically simulated patterns, which supports $C_{70} \subset$**UNMB** adduct formation in 1 : 1 host guest stoichiometry. In fact, in comparison to $C_{60} \subset$**UNMB**, the ESI-MS data showed mainly peaks corresponding to $C_{70} \subset$**UNMB** along with a trace quantity of the free host. This undoubtedly suggests the partial dissociation of $C_{70} \subset$**UNMB** over the ionization period and advocates for the stronger binding ability of **UNMB** for C_{70} as compared to C_{60} (Fig. 6a).

In line with this, we employed UV visible absorption spectroscopy to characterize the host–guest complexation. The UV-Vis absorption spectrum of ligand L^{un} in chloroform showed two absorption bands at λ_{max} 245 and 303 nm, which are due to π–π* transition (Fig. S23†). Meanwhile, the electronic absorption spectrum of **UNMB** displayed two absorption bands at λ_{max} 232 and 308 nm that can be ascribed to the π–π* transition originating from the L^{un} units (Fig. 7). The presence of additional broad bands at around λ_{max} = 362 and 520 nm is owing to **C60**$\subset$**UNMB**, and a strong absorption band at λ_{max} = 361 nm along with a broad band around λ_{max} = 473 nm is due to $C_{70} \subset$**UNMB** in the respective UV-visible absorption spectrum. This truly speaks for the binding of fullerenes with the host **UNMB** (Fig. 7).[23]

After establishing the C_{60}/C_{70}-**UNMB** host–guest complexation qualitatively using NMR, ESI-MS and UV-vis analysis, the binding constants for their formation were determined by UV-vis titrations. Because of the insolubility of fullerenes in acetonitrile, stock solutions (1 mM) of the fullerenes were prepared in toluene. An acetonitrile solution (10 μM) of **UNMB** was titrated with the required amount of fullerene in toluene (Fig. S24 and S26†). Changes in absorbance at λ_{max} 306 nm were plotted against the number of equivalents of C_{60}/C_{70} added, which suggested the formation of a 1 : 1 inclusion complex in both cases (Fig. S24 and S26†). The Benesi–Hildebrand plots (B–H plots)[24] were used to calculate the binding constants, which were roughly found to be 7.15×10^5 M^{-1} for $C_{70} \subset$**UNMB**
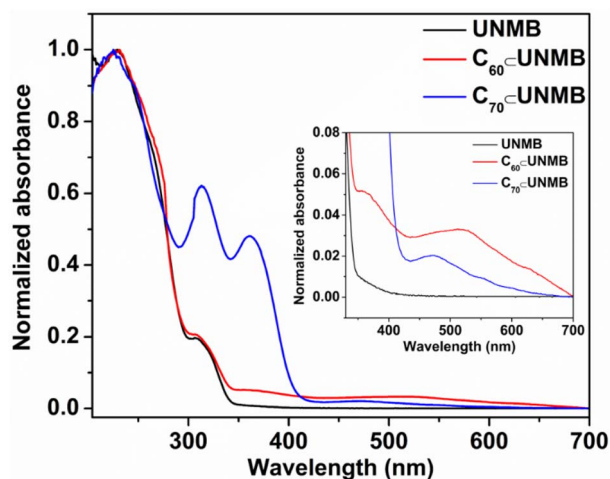

Fig. 7 Absorption spectra of UNMB, $C_{60} \subset$UNMB and $C_{70} \subset$UNMB at room temperature in acetonitrile (10^{-5} M solution). Inset: enlarged UV-vis spectra of UNMB, $C_{60} \subset$UNMB, and $C_{70} \subset$UNMB showing the absorption band due to encapsulated fullerenes.

(Fig. S24 and S25†) and 2.83×10^4 M^{-1} for $C_{60} \subset UNMB$ (Fig. S26 and S27†), which matches well with the literature reports.[18c]

Many attempts were made to grow suitable single crystals of fullerene$\subset$**UNMB** for SC-XRD diffraction, but they remained unsuccessful. Therefore, to obtain a clear idea about the host–guest interactions between the host **UNMB** and guest fullerenes, we did energy optimization of these host–guest complexes using the PM6 semiempirical method in the ground state. The optimized structure of the inclusion complexes revealed that fullerenes C_{60} and C_{70} fit perfectly within the pocket of host **UNMB** (Fig. S28†). The distance between the walls of the **UNMB** and C_{60} surface is $\sim$3.3 Å, whereas those of the C_{70} surface are $\sim$3.3 and 3.5 Å based on the two orientations of C_{70}. The obtained values lie within the range of the required length for efficient π–π interaction between the host and guest.[25] Furthermore, single point energy was computed by employing the DFT method for $C_{70} \subset UNMB$ and $C_{60} \subset UNMB$. These theoretical studies exhibited that the host–guest complexation of $C_{70} \subset UNMB$ is energetically more stable than that of $C_{60} \subset UNMB$. Thus, theoretical studies support the stronger affinity of **UNMB** towards C_{70} found by the association constant values.

Selective extraction of C_{70} from a C_{60}/C_{70} mixture

The stronger binding ability of **UNMB** for C_{70} over C_{60} suggested by ESI-MS and the association constant values is an exciting finding, which gave us the idea to examine the selective binding ability of **UNMB** for the selective extraction of one fullerene from a mixture of C_{60}/C_{70}. Such extraction is very challenging due to the poor solubility of fullerenes in common solvents. To do this, first, a competitive inclusion experiment was performed. To an acetonitrile solution of **UNMB**, an equimolar mixture of C_{60} and C_{70} (2 equiv. of each) was added, and the mixture was heated at 55 °C for 12 h under stirring. The resulting deep purple supernatant was analyzed by ESI-MS, which exhibited the spectral features of $C_{70} \subset UNMB$ (Fig. 8d). Furthermore, an acetonitrile solution of $C_{70} \subset UNMB$ was treated with 2 equivalents of solid C_{60} at 55 °C for 12 h. The ESI-MS spectrum of the so-obtained deep purple solution showed the characteristic pattern of $C_{70} \subset UNMB$ (Fig. 8e). Next, we did this experiment in the reverse manner, and 2 equivalents of solid C_{70} were added to the violet acetonitrile solution of $C_{60} \subset UNMB$ and stirred at 55 °C for 12 h. This again gave a deep purple solution that showed the ESI-MS spectral data of $C_{70} \subset UNMB$ (Fig. 8f). Thus, the C_{70} introduced into the $C_{60} \subset UNMB$ solution replaces the bound C_{60}, but C_{60} could not substitute the bound C_{70} from the cavity of **UNMB**. Therefore, above experiments also confirm that **UNMB** has a stronger binding tendency towards C_{70} than C_{60}.

To investigate whether **UNMB** has the overall ability to extract C_{70} from a C_{70}/C_{60} mixture, an equimolar mixture of C_{70}/C_{60} was treated with 1 mL (10 mg) of an acetonitrile solution of **UNMB** and heated at 55 °C with stirring for 12 h. The centrifuged acetonitrile solution containing predominately $C_{70} \subset UNMB$ was evaporated, and the brown solid thus obtained was treated with 0.5 mL of toluene overnight with stirring at

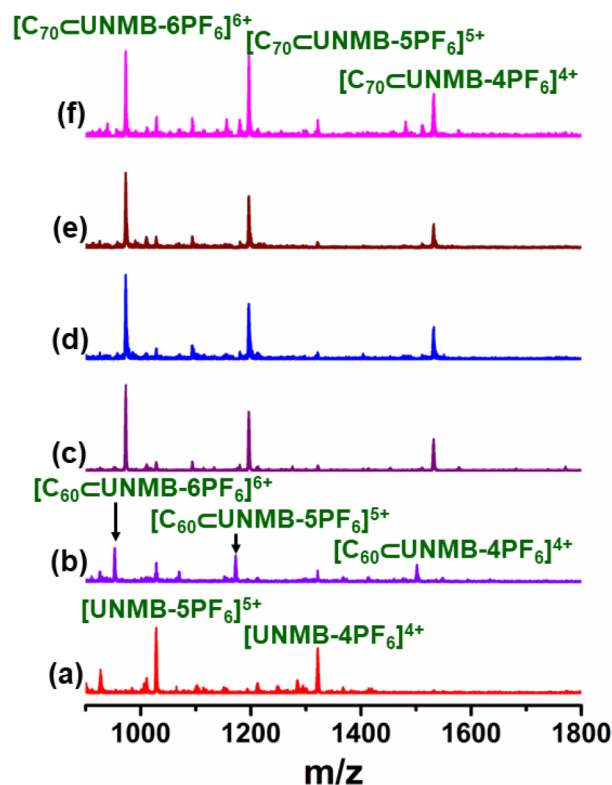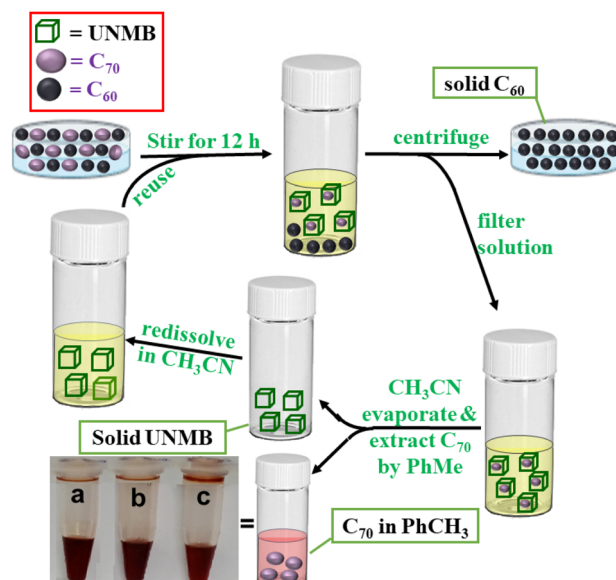**Fig. 8** Partial ESI-MS spectra of (a) UNMB, (b) $C_{60} \subset UNMB$, (c) $C_{70} \subset UNMB$, and (d) UNMB treated with an equimolar (2 eqv. each) mixture of C_{60} and C_{70}, after (e) treatment of $C_{70} \subset UNMB$ with C_{60}, and after (f) treatment of C_{70} with $C_{60} \subset UNMB$.

Scheme 2 Schematic presentation of the separation of fullerene C_{70} from a mixture of C_{60} and C_{70} by UNMB. (Inset picture shows a, b and c labelled vials containing toluene solutions of extracted C_{70} after the 1st, 2nd and 3rd cycles, respectively).

room temperature. The resulting suspension was centrifuged, and the supernatant was investigated by UV-vis analysis. The absorption spectrum of the supernatant in toluene exhibited the absorption profile corresponding to C_{70} (Fig. S29†). Thus, the **UNMB** barrel is found to be a potential receptor for the separation of fullerene C_{70} from its homologue C_{60} (Scheme 2). This is a very stimulating finding as most of the reported fullerene receptors suffer from strong binding without any selectivity and once the guests are bound, their removal is difficult.

The solid residue in the acetonitrile showed an ESI-MS pattern very similar to that of the as-synthesized **UNMB**, along with the good isotopic distribution patterns of several charge fragments (Fig. S30†). This is a fascinating observation that prompted us to check the reusability of barrel **UNMB** as a C_{70} extracting agent. We found that **UNMB** can be reused for the extraction of C_{70} with high purity for three cycles.

Conclusions

In conclusion, we have designed and synthesized an unsymmetrical tetratopic ligand that has two different donor groups (pyridine/imidazole). Its self-assembly with a *cis*-Pd(II) acceptor in a 1:2 molar ratio yielded a low symmetry tetrafacial molecular barrel $\mathbf{M_8L^{un}_4}$ (**UNMB**). The formation of an isomeric molecular barrel (HHTT) was suggested by NMR studies in solution and by the solid-state single-crystal X-ray structure analysis. **UNMB** has two large open windows and a large cavity enclosed by aromatic panels from the unsymmetrical ligands. These features make it a suitable host for binding with large guests like C_{70} and C_{60} through noncovalent interactions (π–π interaction) between the aromatic panels of the barrel and the fullerenes. Encapsulation of fullerenes resulted in an increase in the solubility of C_{60}/C_{70} in acetonitrile, which otherwise are insoluble in the absence of **UNMB**. ESI-MS analysis revealed the formation of 1:1 host–guest inclusion complexes for C_{70} and C_{60}, which was further supported by UV-vis titration experiments. UV-vis titration experiments and competitive guest uptake experiments corroborated that **UNMB** has stronger binding affinity towards C_{70} over its spherical analogue C_{60}, which enabled it to exclusively form a $\mathbf{C_{70} \subset UNMB}$ inclusion complex from a mixture of C_{60} and C_{70}. This preferential binding ability of **UNMB** for C_{70} over C_{60} was employed to separate C_{70} from a mixture of C_{60}/C_{70} with high purity. Moreover, the encapsulated fullerene in pure form was extracted using toluene and the recovered **UNMB** was reused for C_{70} separation for up to three cycles.

Data availability

All data (NMR, ESI-MS) are provided in the ESI,† and additional data will be available upon request.

Author contributions

P. S. M. and D. P. designed the project and devised the experiments. D. P. carried out the experimental work, analysed the

data, optimized the structures, and carried out the theoretical calculations. J. K. C. collected and solved the crystallographic data. All the authors contributed to the writing of the manuscript.

Conflicts of interest

There are no conflicts to declare.

Acknowledgements

References

1 S. E. Ahnert, J. A. Marsh, H. Hernández, C. V. Robinson and S. A. Teichmann, *Science*, 2015, **350**, aaa2245.

2 (*a*) J. E. M. Lewis, A. Tarzia, A. J. P. White and K. E. Jelfs, *Chem. Sci.*, 2020, **11**, 677–683; (*b*) W. Chen, X. Li, C. Liu, J. He, M. Qi, Y. Sun, B. Shi, H. Sepehrpour, H. Li, W. Tian and P. J. Stang, *Proc. Natl. Acad. Sci. U. S. A.*, 2020, **117**, 30942–30948; (*c*) Z. Cui, Q. S. Mu, X. Gao and G. X. Jin, *J. Am. Chem. Soc.*, 2023, **145**, 725–731; (*d*) Y. Hashimoto, Y. Katagiri, Y. Tanaka and M. Yoshizawa, *Chem. Sci.*, 2023, **14**, 14211–14216; (*e*) H.-Y. Lin, Y.-T. Wang, X. Shi, H.-B. Yang and L. Xu, *Chem. Soc. Rev.*, 2023, **52**, 1129–1154; (*f*) M. Yuasa, R. Sumida, Y. Tanaka and M. Yoshizawa, *Chem.–Eur. J.*, 2022, **28**, e202104101; (*g*) Y. Zhu, H. Jiang, W. Wu, X.-Q. Xu, X.-Q. Wang, W.-J. Li, W.-T. Xu, G. Liu, Y. Ke, W. Wang and H.-B. Yang, *Nat. Commun.*, 2023, **14**, 5307.

3 (*a*) J. Liu, T. Luo, Y. Xue, L. Mao, P. J. Stang and M. Wang, *Angew. Chem., Int. Ed.*, 2021, **60**, 5429–5435; (*b*) S. Pullen, J. Tessarolo and G. H. Clever, *Chem. Sci.*, 2021, **12**, 7269–7293; (*c*) B. Shi, P. Qin, Y. Chai, W.-J. Qu, L. Shangguan, Q. Lin, Y.-M. Zhang, Y. Sun, F. Huang and P. J. Stang, *Inorg. Chem.*, 2022, **61**, 8090–8095; (*d*) Y. Wang, Y. Zhang, Z. Zhou, R. T. Vanderlinden, B. Li, B. Song, X. Li, L. Cui, J. Li, X. Jia, J. Fang, C. Li and P. J. Stang, *Nat. Commun.*, 2020, **11**, 2727; (*e*) M. J. Wiester, P. A. Ulmann and C. A. Mirkin, *Angew. Chem., Int. Ed.*, 2011, **50**, 114–137; (*f*) H. N. Zhang and G. X. Jin, *Angew. Chem., Int. Ed.*, 2023, **62**, e202313605.

4 (*a*) R. Chakrabarty, P. S. Mukherjee and P. J. Stang, *Chem. Rev.*, 2011, **111**, 6810–6918; (*b*) Y. Gu, E. A. Alt, H. Wang, X. Li, A. P. Willard and J. A. Johnson, *Nature*, 2018, **560**, 65–69; (*c*) J. M. Lehn, *Science*, 2002, **295**, 2400–2403; (*d*) S. R. Seidel and P. J. Stang, *Acc. Chem. Res.*, 2002, **35**, 972–983; (*e*) L. Tian, C. Wang, H. Zhao, F. Sun, H. Dong, K. Feng, P. Wang, G. He and G. Li, *J. Am. Chem. Soc.*, 2021, **143**, 8631–8638; (*f*) B. Woods, R. D. M. Silva, C. Schmidt, D. Wragg, M. Cavaco, V. Neves, V. F. C. Ferreira, L. Gano, T. S. Morais, F. Mendes, J. D. G. Correia and A. Casini, *Bioconjugate Chem.*, 2021, **32**, 1399–1408; (*g*) Y. Xue, X. Hang, J. Ding, B. Li, R. Zhu, H. Pang and Q. Xu,

Catalysis within coordination cages, *Coord. Chem. Rev.*, 2021, **430**, 213656.

5 (a) P. Howlader, E. Zangrando and P. S. Mukherjee, *J. Am. Chem. Soc.*, 2020, **142**, 9070–9078; (b) A. Platzek, S. Juber, C. Yurtseven, S. Hasegawa, L. Schneider, C. Drechsler, K. E. Ebbert, R. Rudolf, Q. Q. Yan, J. J. Holstein, L. V. Schäfer and G. H. Clever, *Angew. Chem., Int. Ed.*, 2022, **61**, e202209305; (c) H. P. Ryan, C. J. E. Haynes, A. Smith, A. B. Grommet and J. R. Nitschke, *Adv. Mater.*, 2021, **33**, e2004192; (d) T. R. Schulte, J. J. Holstein and G. H. Clever, *Angew. Chem., Int. Ed.*, 2019, **58**, 5562–5566; (e) D. Zhang, T. K. Ronson and J. R. Nitschke, Functional Capsules *via* Subcomponent Self-Assembly, *Acc. Chem. Res.*, 2018, **51**, 2423–2436.

6 (a) T. R. Li, G. Piccini and K. Tiefenbacher, *J. Am. Chem. Soc.*, 2023, **145**, 4294–4303; (b) I. Némethová, D. Schmid and K. Tiefenbacher, *Angew. Chem., Int. Ed.*, 2023, **62**, e202218625; (c) Y. Tsunoda, M. Takatsuka, R. Sekiya and T. Haino, *Angew. Chem., Int. Ed.*, 2017, **56**, 2613–2618; (d) J. Xie, H. J. Peng, J. Q. Huang, W. T. Xu, X. Chen and Q. Zhang, *Angew. Chem., Int. Ed.*, 2017, **56**, 16223–16227; (e) Y. Yang, X. Jing, Y. Shi, Y. Wu and C. Duan, *J. Am. Chem. Soc.*, 2023, **145**, 10136–10148; (f) X. Fu, X. Lin, X. Ren, H. Cong, C. Liu and J. Huang, *Chin. Chem. Lett.*, 2021, **32**, 565–568; (g) Z. Wang, H. F. Su, Y. Z. Tan, S. Schein, S. C. Lin, W. Liu, S. A. Wang, W. G. Wang, C. H. Tung, D. Sun and L. S. Zheng, *Proc. Natl. Acad. Sci. U. S. A.*, 2017, **114**, 12132–12137; (h) B.-L. Han, Z. Wang, R. K. Gupta, L. Feng, S. Wang, M. Kurmoo, Z.-Y. Gao, S. Schein, C.-H. Tung and D. Sun, *ACS Nano*, 2021, **15**, 8733–8741; (i) H. Han, L. Kan, P. Li, G. Zhang, K. Li, W. Liao, Y. Liu, W. Chen and C. T. Hu, *Sci. China: Chem.*, 2021, **64**, 426–431.

7 (a) R. Banerjee, D. Chakraborty and P. S. Mukherjee, *J. Am. Chem. Soc.*, 2023, **145**, 7692–7711; (b) P. Bhandari, R. Modak, S. Bhattacharyya, E. Zangrando and P. S. Mukherjee, *JACS Au*, 2021, **1**, 2242–2248; (c) I. A. Bhat, R. Jain, M. M. Siddiqui, D. K. Saini and P. S. Mukherjee, *Inorg. Chem.*, 2017, **56**, 5352–5360; (d) P. Das, A. Kumar, P. Howlader and P. S. Mukherjee, *Chem.–Eur. J.*, 2017, **23**, 12565–12574; (e) P. Howlader, B. Mondal, P. C. Purba, E. Zangrando and P. S. Mukherjee, *J. Am. Chem. Soc.*, 2018, **140**, 7952–7960; (f) R. Saha, A. Devaraj, S. Bhattacharyya, S. Das, E. Zangrando and P. S. Mukherjee, *J. Am. Chem. Soc.*, 2019, **141**, 8638–8645.

8 (a) D. P. Giannopoulos, A. Thuijs, W. Wernsdorfer, M. Pilkington, G. Christou and T. C. Stamatatos, *Chem. Commun.*, 2014, **50**, 779–781; (b) P. Howlader, P. Das, E. Zangrando and P. S. Mukherjee, *J. Am. Chem. Soc.*, 2016, **138**, 1668–1676; (c) Y. Kim, W. Li, S. Shin and M. Lee, *Acc. Chem. Res.*, 2013, **46**, 2888–2897; (d) R. Saha, B. Mondal and P. S. Mukherjee, *Chem. Rev.*, 2022, **122**, 12244–12307.

9 (a) J. E. M. Lewis and J. D. Crowley, *ChemPlusChem*, 2020, **85**, 815–827; (b) J. E. M. Lewis, A. Tarzia, A. J. P. White and K. E. Jelfs, *Chem. Sci.*, 2019, **11**, 677–683; (c) D. Prajapati, P. Bhandari, N. Hickey and P. S. Mukherjee, *Inorg. Chem.*, 2023, **62**, 9230–9239; (d) S. Pullen, J. Tessarolo and G. H. Clever, *Chem. Sci.*, 2021, **12**, 7269–7293; (e)

R. G. Siddique, K. S. A. Arachchige, H. A. Al-Fayaad, J. D. Thoburn, J. C. McMurtrie and J. K. Clegg, *Angew. Chem., Int. Ed.*, 2022, **61**, e202115555; (f) D. Prajapati, P. Bhandari, E. Zangrando and P. S. Mukherjee, *Chem. Sci.*, 2024, **15**, 3616–3624; (g) R. G. Siddique, J. J. Whittaker, H. A. Al-Fayaad, J. C. McMurtrie and J. K. Clegg, *Dalton Trans.*, 2023, **52**, 13487–13491.

10 (a) D. Bardhan and D. K. Chand, *Chem.–Eur. J.*, 2019, **25**, 12241–12269; (b) W. M. Bloch and G. H. Clever, *Chem. Commun.*, 2017, **53**, 8506–8516; (c) S. Pullen and G. H. Clever, *Acc. Chem. Res.*, 2018, **51**, 3052–3064.

11 (a) W.-X. Gao, H.-N. Zhang and G.-X. Jin, *Coord. Chem. Rev.*, 2019, **386**, 69–84; (b) M. Hardy and A. Lützen, *Chem.–Eur. J.*, 2020, **26**, 13332–13346; (c) H. Li, Z.-J. Yao, D. Liu and G.-X. Jin, *Coord. Chem. Rev.*, 2015, **293–294**, 139–157; (d) L. S. Lisboa, D. Preston, C. J. McAdam, L. J. Wright, C. G. Hartinger and J. D. Crowley, *Angew. Chem., Int. Ed.*, 2022, **61**, e202201700; (e) Z. Zhou, J. Liu, T. W. Rees, H. Wang, X. Li, H. Chao and P. J. Stang, *Proc. Natl. Acad. Sci. U. S. A.*, 2018, **115**, 5664–5669.

12 (a) R. J. Li, A. Marcus, F. Fadaei-Tirani and K. Severin, *Chem. Commun.*, 2021, **57**, 10023–10026; (b) R. J. Li, A. Tarzia, V. Posligua, K. E. Jelfs, N. Sanchez, A. Marcus, A. Baksi, G. H. Clever, F. Fadaei-Tirani and K. Severin, *Chem. Sci.*, 2022, **13**, 11912–11917; (c) S. S. Mishra, S. V. K. Kompella, S. Krishnaswamy, S. Balasubramanian and D. K. Chand, *Inorg. Chem.*, 2020, **59**, 12884–12894; (d) D. Ogata and J. Yuasa, *Angew. Chem., Int. Ed.*, 2019, **58**, 18424–18428; (e) D. Preston and J. D. Evans, *Angew. Chem., Int. Ed.*, 2023, **62**, e202314378.

13 (a) H. W. Kroto, J. R. Heath, S. C. O'Brien, R. F. Curl and R. E. Smalley, *Nature*, 1985, **318**, 162–163; (b) P. W. Stephens, D. Cox, J. W. Lauher, L. Mihaly, J. B. Wiley, P.-M. Allemand, A. Hirsch, K. Holczer, Q. Li, J. D. Thompson and F. Wudl, *Nature*, 1992, **355**, 331–332; (c) Z. Yao and K. C. Tam, *Macromol. Rapid Commun.*, 2011, **32**, 1863–1885.

14 M. Prato, *J. Mater. Chem.*, 1997, **7**, 1097–1109.

15 Y. Iwasa, *Nature*, 2010, **466**, 191–192.

16 (a) G. Dennler, M. C. Scharber and C. J. Brabec, *Adv. Mater.*, 2009, **21**, 1323–1338; (b) S. K. Park, J. H. Kim and S. Y. Park, *Adv. Mater.*, 2018, **30**, 1704759.

17 (a) H. Aoshima, S. Yamana, S. Nakamura and T. Mashino, *J. Toxicol. Sci.*, 2010, **35**, 401–409; (b) H. Kazemzadeh and M. Mozafari, *Drug Discovery Today*, 2019, **24**, 898–905; (c) G.-F. Liu, M. Filipović, I. Ivanović-Burmazović, F. Beuerle, P. Witte and A. Hirsch, *Angew. Chem., Int. Ed.*, 2008, **47**, 3991–3994.

18 (a) C. García-Simón, M. Costas and X. Ribas, *Chem. Soc. Rev.*, 2016, **45**, 40–62; (b) J. Pfeuffer-Rooschüz, S. Heim, A. Prescimone and K. Tiefenbacher, *Angew. Chem., Int. Ed.*, 2022, **61**, e202209885; (c) P. C. Purba, M. Maity, S. Bhattacharyya and P. S. Mukherjee, *Angew. Chem., Int. Ed.*, 2021, **60**, 14109–14116.

19 (a) J. Theobald, M. Perrut, J. V. Weber, E. Millon and J. F. Muller, *Sep. Sci. Technol.*, 1995, **30**, 2783–2819; (b) C. Yeretzian, J. B. Wiley, K. Holczer, T. M. Su, S. L. Nguyen,

R. B. Kaner and R. L. Whetten, *J. Phys. Chem.*, 1993, **97**, 10097–10101.

20 A. Hirsch and M. Brettreich, *Fullerenes: Chemistry and Reactions*, Wiley-VCH, Weinheim, Germany, 2005.

21 (*a*) J. L. Atwood, G. A. Koutsantonis and C. L. Raston, *Nature*, 1994, **368**, 229–231; (*b*) S. Bera, S. Das, M. Melle-Franco and A. Mateo-Alonso, *Angew. Chem., Int. Ed.*, 2023, **62**, e202216540; (*c*) W. Meng, B. Breiner, K. Rissanen, J. D. Thoburn, J. K. Clegg and J. R. Nitschke, *Angew. Chem., Int. Ed.*, 2011, **50**, 3479–3483; (*d*) K. Tashiro and T. Aida, *Chem. Soc. Rev.*, 2007, **36**, 189–197; (*e*) L. Wang, G. T. Wang, X. Zhao, X. K. Jiang and Z. T. Li, *J. Org. Chem.*, 2011, **76**, 3531–3535; (*f*) M. Zhang, H. Xu, M. Wang, M. L. Saha, Z. Zhou, X. Yan, H. Wang, X. Li, F. Huang, N. She and P. J. Stang, *Inorg. Chem.*, 2017, **56**, 12498–12504.

22 D. Aragão, J. Aishima, H. Cherukuvada, R. Clarken, M. Clift, N. P. Cowieson, D. J. Ericsson, C. L. Gee, S. Macedo, N. Mudie, S. Panjikar, J. R. Price, A. Riboldi-Tunnicliffe, R. Rostan, R. Williamson and T. T. Caradoc-Davies, *J. Synchrotron Radiat.*, 2018, **25**, 885–891.

23 G. Orlandi and F. Negri, *Photochem. Photobiol. Sci.*, 2002, **1**, 289–308.

24 (*a*) Y. Shi, K. Cai, H. Xiao, Z. Liu, J. Zhou, D. Shen, Y. Qiu, Q.-H. Guo, C. Stern, M. R. Wasielewski, F. Diederich, W. A. Goddard III and J. F. Stoddart, *J. Am. Chem. Soc.*, 2018, **140**, 13835–13842; (*b*) P. Thordarson, *Chem. Soc. Rev.*, 2011, **40**, 1305–1323.

25 (*a*) J.-H. Deng, J. Luo, Y.-L. Mao, S. Lai, Y.-N. Gong, D.-C. Zhong and T.-B. Lu, *Sci. Adv.*, 2020, **6**, eaax9976; (*b*) C. Janiak, *J. Chem. Soc., Dalton Trans.*, 2000, 3885–3896.